17th CIRP Conference on Modelling of Machining Operations

Machining induced damage in orthogonal cutting of UD composites: FEA based assessment of Hashin and Puck criteria

F. Cepero-Mejias[a,b,c,*], V.A. Phadnis[d], J.L. Curiel-Sosa[b,c]

[a]*Industrial Doctorate Centre in Machining Science, The University of Sheffield, Sir Frederick Mappin Building, Mappin Street, S1 3JD Sheffield, United Kingdom.*
[b]*Computer-Aided Aerospace & Mechanical Engineering (CA2M) Research Group, Sir Frederick Mappin Building, Mappin Street, S1 3JD Sheffield, United Kingdom.*
[c]*Department of Mechanical Engineering, The University of Sheffield, Sir Frederick Mappin Building, Mappin Street, S1 3JD Sheffield, United Kingdom.*
[d]*AMRC with Boeing, Advanced Manufacturing Park, Wallis Way, Catcliff, Rotherham, S605TZ, United Kingdom.*

Abstract

FE models offer a promising virtual alternative to study machining responses of composites, thereby allowing an informed selection of favorable cutting parameters. Appropriate mathematical schemes are needed to predict damage initiation in fibrous composites; Hashin and Puck failure criteria are the most commonly used for this purpose. This work focusses on the assessment of these criteria to predict ply-level damage in orthogonal cutting of unidirectional composites. A novel algorithm accounting for strain-softening after damage initiation is also proposed. Efficacy of the developed FE model is shown by simulating effects of the cutter tool on the damage of underlying workpiece.

© 2019 The Authors. Published by Elsevier B.V.
Peer-review under responsibility of the scientific committee of The 17th CIRP Conference on Modelling of Machining Operations

Keywords: Composite ; Damage ; Hashin failure criteria ; Orthogonal cutting ; Puck failure criteria ; Finite element

1. Introduction

In last few years, polymer matrix composites (PMCs) are being widely used in various industrial applications due to their exceptional strength-to-weight properties and excellent fatigue and corrosion resistance. This trend is especially encouraging in aerospace industry where Boeing 787 recently used more than 50% by weight of PMCs to construct the mainframe components, eliminating 1,500 aluminium sheets and 40,000-50,000 fasteners per section making the aircraft much lighter and therefore, fuel efficient [1].

PMCs though are manufactured to a near-net shape, machining operations are needed to meet strict assembly tolerances and produce holes for assembly purpose. However, abrasive fibres and tough polymer matrices pose challenges in achieving desired cut surface finish. The low thermal conductivity of thermoset resins means, in high-speed machining applications the process-heat gets attracted more to metallic cutting tool contributing to its accelerated thermo-mechanical wear. Consequently, the worn cutting tools, during cutting, bend highly elastic fibres ahead of the tool tip instead of shearing them away, resulting in higher degree of surface and sub-surface damage. In addition, incorrect choice of cutting parameters gives rise to several damage mechanisms such as delamination, fibre-matrix debonding and matrix crushing [2, 3]. In such scenario, a large number of machining trials are generally needed to understand the effect of critical process variables on the cut surface quality, and machining-induced damage that could result in part-rejection.

Owing to the high cost associated with aerospace-grade composites and modern cutting tools, this exercise could be quite expensive and laborious. Finite-element (FE) models of machining of composites could be a cost-effective alternative when validated using the experimental data. FE models emulating composite machining process have been used to study various machining responses recently.

Lasri et al. [4], while studying mechanics of chip removal using FE model of orthogonal machining of CFRP composite, concluded that the chip removal mechanism is mainly taking place at fibre-matrix interface. A gradual chip length reduction for fibre orientations ranging from 0° to 90° was evident to support the conclusion. In another study using FEA, fo-

---

cused on modelling of machining the epoxy-based composites impregnated with carbon – and glass – fibres, Santiuste et al. [5] determined that upon machining CFRP experience a brittle fracture with low induced damage, while GFRP shows a more ductile behaviour with higher sub-surface damage. This helped to drawn an insight in selection of appropriate cutting parameters in a case where hybrid (CFRP/GFRP) composites are machined. The effect of fibre orientation, rake angle and depth-of-cut on internal damage propagation and cutting forces was investigated by Zenia et al. [6]. The FE study concluded that the high fibre orientations and high depths-of-cut result in increased machining induced damage and cutting forces, while increment in rake angle reduce these responses – highlighting the importance of suitable cutter geometry.

An extensive review of present machining FE works reveals that several authors have studied the effect of cutting parameters on the laminate sub-surface damage. However, in most cases these studies are not supported with the experimental or analytical evidences leading to uncertainty on the overall predictability and robustness of these models. Therefore, development of FE model of machining of composites, thoroughly validated using experimental results, is required to enhance the ability of prediction.

Currently, a damage algorithm proposed by Hashin [7, 8] to determine damage initiation and a subsequent linear energy based softening available in Abaqus/Explicit commands is widely used to model underlying fibre/matrix damage in machining simulations. Nevertheless, Hashins criteria is quite conservative in prediction of initation of matrix damage under compressive loads [9]. This introduces critical errors in numerical results, as these damage modes are significant in machining applications [5]. Besides, traditional element-deletion methods are commonly employed to model material removal upon damage and thereby avoid numerical instability arising from excessive distortion of meshed elements. These methods do not allow damage propagation in a physical manner, predicting much lower damage than that of observed in experimental trials. Hence, more sophisticated mathematical models accounting for composite fracture and damage mechanisms should be developed to improve the underlying damage predictions [10].

This article focusses on the 2D FE simulation of orthogonal cutting of composites taking into account effect of various fibre orientations and change of cutter geometry. Two numerical algorithms - Hashin-Rotem and Puck failure criteria, widely used in FE modelling community to model onset of damage in stressed composite structures, are considered to comprehend their effectiveness and de-merits when applied to composite machining application. Damage propagation is modelled using a linear physical energy based softening and imposing a threshold damage level. This helps to avoid element distortion problems as highlighted before, and takes into account composite structures residual strength. Spring back phenomenon, often observed in composite machining is also considered to enhance thrust force and sub-surface damage predictions. Developed FE models are validated by comparing FE results with experimental machining force data as well as optical induced damage measurements published elsewhere [11].

Nomenclature

FE	Finite element
PMC	Polymer matrix composite
GFRP	Glass fibre reinforced polymer
σ_{ij}	Stress vector values in directions "i" and "j"'
E_1, E_2	Young modulus in fibre and transverse directions
G_{12}, ν_{12}	Shear laminate modulus and poisson coefficient
X_T, X_C	Fibre tensile and compressive strength
Y_T, Y_C	Matrix tensile and compressive strength
S	Shear laminate strength
$p_{\perp\parallel}^{(+)}$	Slope of the fracture envelope (normal stress - longitudinal/transverse shear stress) curve in traction states when normal stress is 0
$R_{\perp}^{(+)A}$	Fracture resistance of the fracture plane due to transverse stresses
$R_{\perp\parallel}^{A}$	Fracture resistance of the fracture plane due longitudinal/transverse shear stresses
$R_{\perp\perp}^{A}$	Fracture resistance of the fracture plane due to transverse/transverse shear stresses
$\delta_{I,eq}$	Equivalent displacement associated to a damage mode
$\delta_{I,eq}^{0}$	Equivalent displacement associated to a damage mode when it is 0
$\sigma_{I,eq}^{0}$	Equivalent stress associated to a damage mode when it is 0
$\delta_{I,eq}^{f}$	Equivalent displacement associated to a damage mode when it is 1
G_{I}^{C}	Critical fracture toughness associated to a damage mode

2. FE model characteristics

Several 2D FEM plane stress analyses are conducted in the numerical software package Abaqus/Explicit. Same machining configuration employed in Bhatnagar et al. [11] trials is implemented to validate the FE model, refer to Table 3. Tool is treated as a solid rigid to reduce the high computational time required for these kind of FE models. GFRP mechanical and strength material properties simulated are listed in Tables 1 and 2, respectively.

Table 1. GFRP composite mechanical properties.

Material	$E_1(GPa)$	$E_2(GPa)$	$G_{12}(GPa)$	ν_{12}
GFRP [5]	48	12	6	0.28

Table 2. GFRP composite strength properties.

Material	$X_T(MPa)$	$X_C(MPa)$	$Y_T(MPa)$	$Y_C(MPa)$	$S(MPa)$
GFRP [5]	1200	800	59	128	25

Table 3. Cutting parameters simulated.

Cutting variables	Simulated machining configuration
Rake angle (α)	5°
Relief angle (β)	6°
Tool edge radius (μm)	50
Depth of cut (mm)	0.2
Cutting speed (mm/s)	8.33
Fibre orientations	0°, 15°, 30°, 45°, 60°, 75° and 90°

2.1. Mesh and geometry considerations

Laminate dimensions are 5 mm long and 3 mm height to accomplish a good compromise between accuracy and computational cost of the numerical predictions. Cutter tool edge is allocated at the middle of long laminate side to faithfully reproduce the usual cutting conditions along the laminate. Boundary conditions are carefully chosen to resemble the real cutting conditions; bottom laminate displacements are fixed, while in lateral laminate sides the horizontal movement is restricted. Quadrilateral CPS4R meshed elements are employed with a minimum size of 10 μm in the zone around the cutter tool tip and a maximum size of 100 μm at the lateral and bottom laminate sites, as illustrated in Fig. 1.
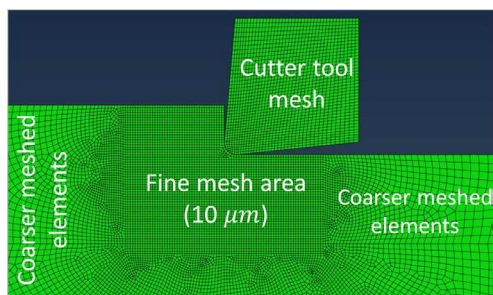
Fig. 1. Mesh zoom of the closed area next to the cutter tool edge.

2.2. Tool-workpiece contact

The contact is simulated using the surface-node surface contact property available in Abaqus/Explicit in-built commands. To model the friction a low constant friction Coulomb coefficient of 0.2 is chosen for every simulated fibre orientation. This consideration is taken to use similar frictional coefficients extracted from Koplev et al. [12] experiments.

3. Damage algorithms

The development of two novel damage algorithms in the modelling of composite machining is performed using an user fortran subroutine VUMAT. Four different damage modes are considered inside stiffness matrix: (1) fibre traction (d_{ft}), (2) fibre compression (d_{fc}), (3) matrix traction (d_{mt}) and (4) matrix compression (d_{mc}). Their implementation in the constitutive

equations of the material is carried out using the same formulation developed by Lapczyk and Hurtado [13].

One of the damage algorithms employ the Hashin-Rotem failure criteria to predict the damage initiation in composite ply. The criteria typically result in over-prediction of damage magnitude, thus leading to a conservative design envelope. In addition, its mathematical formulation does not contain numerical terms which typically aggregate to serious round-off errors (e.g. square roots or denominators approaching zero). This makes criteria attractive for implementation in FE codes. This is inserted in the FE model using damage activation functions for every damage mode (F_I; with $I = \{ft, fc, mt, mc\}$); fibre or matrix damage onset is predicted when one of the damage activation functions achieve a value equal or superior to 1. Hashin-Rotem stress formulation is illustrated below.

- Fibre traction ($\sigma_{11} \geq 0$)

$$F_{ft} = \left(\frac{\sigma_{11}}{X_T} \right) \geq 1 \qquad (1)$$

- Fibre compression ($\sigma_{11} < 0$)

$$F_{fc} = \mid \frac{\sigma_{11}}{X_C} \mid \geq 1 \qquad (2)$$

- Matrix traction ($\sigma_{22} \geq 0$)

$$F_{mt} = \left(\frac{\sigma_{22}}{Y_T} \right)^2 + \left(\frac{\sigma_{12}}{S} \right)^2 \geq 1 \qquad (3)$$

- Matrix compression ($\sigma_{22} < 0$)

$$F_{mc} = \left(\frac{\sigma_{22}}{Y_C} \right)^2 + \left(\frac{\sigma_{12}}{S} \right)^2 \geq 1 \qquad (4)$$

In the another damage algorithm proposed, damage activation functions illustrated in Eqs. 1 and 2 are used to predict fibre damage initiation, while matrix damage initiation is calculated using Puck's failure criteria. This is decided owing sub-surface damage extension is mainly governed by matrix damage modes [4, 5] and Puck's failure criteria offers high capabilities to predict this kind of composite failures [14].

Three matrix damage modes are considered Mode A, Mode B and Mode C in Puck failure criteria. Mode A is associated to the matrix traction damage mode, while Mode B and Mode C are assigned to compression states with high and low shear contribution, respectively. In this work, for simplicity purpose, F_{mt} is calculated using Mode A equation ($F_{mt} = F_{mma}$), while F_{mc} is obtained as the maximum value between Mode B and Mode C ($F_{mc} = max\{F_{mmb}, F_{mmc}\}$). Matrix Puck's failure criteria is formulated as reads.

- Mode A ($\sigma_{22} \geq 0$)

$$F_{mma} = \sqrt{\left(\frac{\sigma_{12}}{R_{\perp\parallel}^A} \right)^2 + \left(1 - \frac{p_{\perp\parallel}^{(+)}}{R_\perp^A} R_\perp^{(+)A} \right)^2 \left(\frac{\sigma_{22}}{R_\perp^{(+)A}} \right)^2} + \frac{p_{\perp\parallel}^{(+)}}{R_{\perp\parallel}^A} \sigma_{22} \geq 1 \qquad (5)$$

- Mode B ($\sigma_{22} < 0$ and $\sigma_{22} > -R_{\perp\perp}^A$)

$$F_{mmb} = \sqrt{\left(\frac{\sigma_{12}}{R^A_{\perp\parallel}}\right)^2 + \left(\frac{p}{R}\right)^2 \sigma^2_{22}} + \left(\frac{p}{R}\right)\sigma_{22} \geq 1 \qquad (6)$$

- Mode C ($\sigma_{22} \leq -R^A_{\perp\perp}$)

$$F_{mmc} = \frac{1}{2\left[1 + \left(\frac{p}{R}\right)R^A_{\perp\perp}\right]}\left[\left(\frac{\sigma_{12}}{R^A_{\perp\parallel}}\right)^2 + \left(\frac{\sigma_{22}}{R^A_{\perp\perp}}\right)^2\right]\frac{R^A_{\perp\perp}}{-\sigma_{22}} \geq 1 \quad (7)$$

For the brevity purpose, Puck's variables definitions are described in the nomenclature of this document. To achieve a better understanding of Puck's failure criteria interested, readers are referred to [15]. Once damage initiation is achieved for a determined damage mode, a linear continuum damage mechanics approach is applied. The damage variables evolution depend upon equivalent displacements ($\delta_{I,eq}$), as shown in Eq. 8.

$$d_I = \frac{\delta^f_{I,eq}\left(\delta_{I,eq} - \delta^0_{I,eq}\right)}{\delta_{I,eq}\left(\delta^f_{I,eq} - \delta^0_{I,eq}\right)} \qquad (8)$$

In the above equation, the initial equivalent displacement ($\delta^0_{I,eq}$) and final equivalent displacement ($\delta^f_{I,eq}$) represents the displacements when damage starts ($d_I = 0$) and the total damage is achieved ($d_I = 1$) in meshed elements. Both expressions are calculated immediately after damage initiation is reached using the equivalent stress ($\sigma_{I,eq}$) and the critical fracture toughness (G^c_I), as shown in Eqs. 9 and 10. These previous variables are explained in more detail in [13]. G^c_I values employed in this work are showcased in Table 4.

$$\delta^f_{I,eq} = \frac{2G^c_I F_I}{\sigma_{I,eq}} \qquad (9)$$

$$\delta^0_{I,eq} = \frac{\delta_{I,eq}}{F_I} \qquad (10)$$

Table 4. Critical fracture toughness values employed

N/mm	G^c_{ft}	G^c_{fc}	G^c_{mt}	G^c_{mc}
G^C_I	10	10	1	1

Finally, a maximum damage of 0.95 is assigned to matrix damage modes (d_{mt} and d_{mc}), while for fibre modes (d_{ft} and d_{fc}), the maximum value allowed is 0.999. This assumption is taken to simulate the residual strength that the matrix of a failure ply still contribute to the adjacent laminate plies [16] and also to avoid element distortion problems [4].

4. Results and discussions

As the main purpose of this work is to assess the machining induced damage, simulations are stopped when chip release is about to occur without considering element deletion. For model

validation purpose, the chip formation is assumed to take place when the numerical cutting force achieve the experimental values measured in Bhatnagar et al. [11] experiments.

Spring back phenomenon, which consider the partial thickness recovery that take place in the laminate after the tool cut the material, is considered in the FE model with the insertion of a progressive cutter tool vertical penetration throughout the thickness; the addition of this factor enhance the numerical thrust force and sub-surface damage predictions, see Figs. 2 and 6. Maximum cutter tool penetration in both are selected around the half or one tool edge radius value as it was investigated by Wang et al. [17], as shown in Fig. 3.
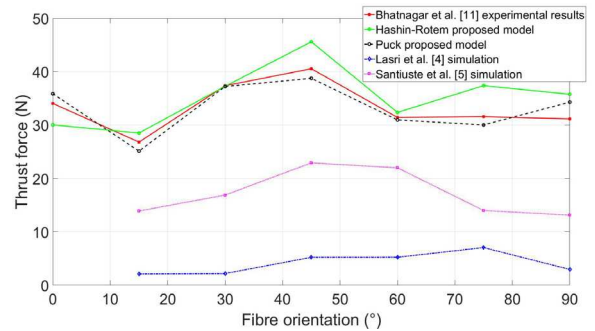
Fig. 2. Experimental and numerical thrust force analysis.

Sub-surface damage is measured as the vertical distance between the lowest point where damage initiation is reached and machined surface. As mention before, matrix damage modes determine the sub-surface damage, owing fibre failure is negligible. Three distinct damage zones are observed: (1) below, (2) behind and (3) in front of the cutting tool tip. In zone 1, both traction and compression damage modes are developed because failure is governed by shear stressed in the boundary region between F_{mt} and F_{mc}. In the case of region 2, matrix traction states are dominant due to the tool-workpiece frictional forces. Matrix compression damage is encountered in region 3, because of the pushing force exerted by the cutting tool. All these arguments are clearly exposed in Fig. 4, showing the position in the stress domain of where composite failure take place in Hashin-Rotem and Puck failure envelopes.

It is observed that both damage models studied predicts sub-surface damage in good agreement with experimental results for low fibre orientations 0°-45°. However, for high fibre orien-
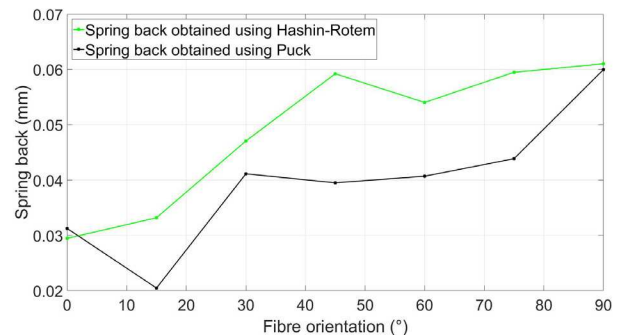
Fig. 3. Calculated Hashin-Rotem and Puck spring back in simulations.
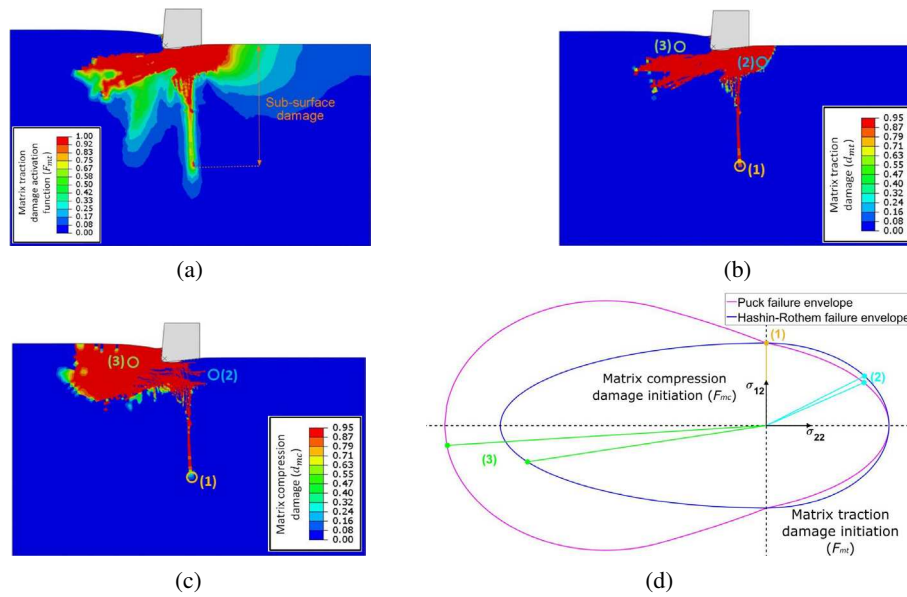
Fig. 4. Sub-surface damage illustration and laminate damage sites analysis for a fibre orientation of 90°: (a) Sub-surface damage determination, (b) Puck d_{mt} representation, (c) Hashin-Rotem d_{mc} representation and (d) Location of damage modes in different laminate sites assessed in Puck and Hashin-Rotem failure envelopes.
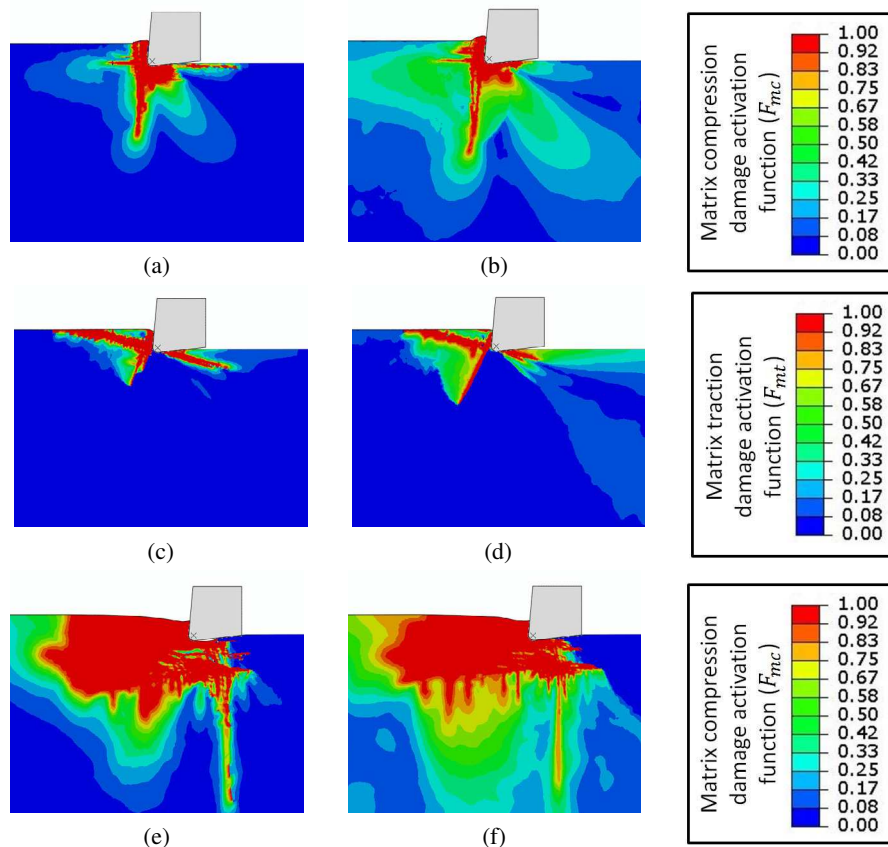
Fig. 5. Representation of sub-surface matrix damage modes propagation through the laminate at the end of simulation time: (a,b) F_{mc} distribution obtained with a fibre orientation of 0° obtained using Hashin-Rotem and Puck criteria, respectively, (c,d) F_{mt} distribution with a fibre orientation of 15° obtained using Hashin-Rotem and Puck criteria, respectively and (e,f) F_{mc} distribution with a fibre orientation of 90° obtained using Hashin-Rotem and Puck criteria, respectively.

tations 60°-90° numerical predictions diverge appreciably from the experimental findings. This fact could be caused because for these fibre orientations the fibre/matrix debonding failure, which is neglected in this work, plays a relevant role incrementing notably the machining induced damage depth. Nevertheless, the numerical results obtained are still valid, as both FE models

predict faithfully the same trend experienced in experimental trials, as shown in Fig. 6.
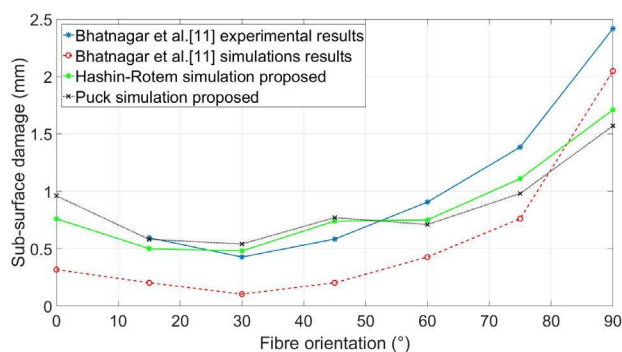
Fig. 6. Sub-surface damage predictions obtained with Hashin-Rotem and Puck and Bhatnagar et al. [11] experimental and numerical results.

It is concluded that the fibre orientation has a remarkable influence on the damage underlying the machined surface. Low fibre orientations, i.e. 15° and 30°, experience a brittle chip fracture with a small sub-surface damage propagation, while for high fibre orientations, i.e. 75° and 90°, chip formation mechanism is remarkably more ductile with higher underlying damage. In the particular case of laminates with a fibre orientation of 0°, the sub-surface damage is remarkably higher than the experienced by low fibre orientation laminates; this fact occurs because of the fibre buckling, which produce along the cutting process, induce a significant increment of the sub-surface damage. This final statements are visualised in Fig. 5, where damage initiation functions F_{mt} and F_{mc} are represented to show the damaged area of laminates with fibre orientations of 0°,15° and 90°.

5. Conclusions

This article develops a novel FEM study in the machining of UD-PMCs with the proposal of two sophisticated composite damage algorithms. Hashin-Rotem and Puck failure criteria in combination with the post-damage treatment applied have demonstrated to be effective predicting the same machining induced damage tendency observe in experimental findings. For fibre orientations between 0°- 45° , the numerical predictions are in accordance with experimental findings, while for fibre orientations in the range of 60°-90° a noticeable discrepancy between numerical and experimental results, is obtained.

This divergence could be explained owing the fibre/matrix debonding – not included in this analysis – might increment notably the prediction of sub-surface damage for high fibre orientations. Additionally, inclusion of spring back phenomenon have been proved to be essential to enhance the numerical thrust force predictions. Future works using these damage algorithms will be developed for predicting the influence of cutting parameters such as rake angle, relief angle, tool wear or depth of cut on the post-machining damage suffered by the workpiece.

References

[1] Boeing, "Boeing 787 Dreamliner," 2018.
[2] C. Zhang, J. L. Curiel-sosa, and T. Quoc, "Meso-scale progressive damage modeling and life prediction of 3D braided composites under fatigue tension loading," *Composite Structures*, vol. 201, no. June, pp. 62–71, 2018.
[3] J. L. Curiel-sosa, B. Tafazzolimoghaddam, and C. Zhang, "Modelling fracture and delamination in composite laminates : Energy release rate and interface stress," *Composite Structures*, vol. 189, no. January, pp. 641–647, 2018.
[4] L. Lasri, M. Nouari, and M. El Mansori, "Modelling of chip separation in machining unidirectional FRP composites by stiffness degradation concept," *Composites Science and Technology*, vol. 69, no. 5, pp. 684–692, 2009.
[5] C. Santiuste, X. Soldani, and M. H. Miguélez, "Machining FEM model of long fiber composites for aeronautical components," *Composite Structures*, vol. 92, no. 3, pp. 691–698, 2010.
[6] S. Zenia, L. Ben Ayed, M. Nouari, and A. Delamézière, "Numerical analysis of the interaction between the cutting forces, induced cutting damage, and machining parameters of CFRP composites," *International Journal of Advanced Manufacturing Technology*, vol. 78, no. 1-4, pp. 465–480, 2015.
[7] Z. Hashin and A. Rotem, "A Fatigue Failure Criterion for Fiber Reinforced Materials," *Journal of Composite Materials*, vol. 7, no. 4, pp. 448–464, 1973.
[8] Z. Hashin, "Failure Criteria for Unidirectional FibreComposites," *Journal of Applied Mechanics*, vol. 47, no. June, pp. 329–334, 1980.
[9] R. Gutkin and S. Pinho, "Review on failure of laminated composites : Experimental perspective and modelling," 2016.
[10] J. L. Curiel Sosa, S. Phaneendra, and J. J. Munoz, "Modelling of mixed damage on fibre reinforced composite laminates subjected to low velocity impact," *International Journal of Damage Mechanics*, vol. 22, no. 3, pp. 356–374, 2013.
[11] N. Bhatnagar, D. Nayak, I. Singh, H. Chouhan, and P. Mahajan, "Determination of machining-induced damage characteristics of fiber reinforced plastic composite laminates," *Materials and Manufacturing Processes*, vol. 19, no. 6, pp. 1009–1023, 2004.
[12] A. Koplev, A. Lystrup, and T. Vorm, "The cutting process, chips, and cutting forces in machining CFRP," *Composites*, vol. 14, no. 4, pp. 371–376, 1983.
[13] I. Lapczyk and J. A. Hurtado, "Progressive damage modeling in fiber-reinforced materials," *Composites Part A: Applied Science and Manufacturing*, vol. 38, no. 11, pp. 2333–2341, 2007.
[14] M. J. Hinton, A. S. Kaddour, and P. D. Soden, "A comparison of the predictive capabilities of current failure theories for composite laminates , judged against experimental evidence," *Composites Science and Technology*, vol. 62, pp. 1725–1797, 2002.
[15] A. Puck and H. Schurmann, "Failure Analysis of Frp Laminates By Means of Physically Based Phenomenological Models *," *Composites Science and Technology*, vol. 3538, no. 96, pp. 1633–1662, 1998.
[16] F. Paris, J. Canas, and J. Marin, *Introduccion al analisis y diseno con materiales compuestos*. Sevilla: Universidad de Sevilla, Escuela Tecnica Superior de Ingenieros, 2008.
[17] X. M. Wang and L. C. Zhang, "An experimental investigation into the orthogonal cutting of unidirectional fibre reinforced plastics," *International Journal of Machine Tools and Manufacture*, vol. 43, no. 10, pp. 1015–1022, 2003.